IET Radar, Sonar & Navigation

Special Issue Call for Papers

Be Seen. Be Cited.
Submit your work to a new IET special issue

Connect with researchers and experts in your field and share knowledge.

Be part of the latest research trends, faster.

Read more

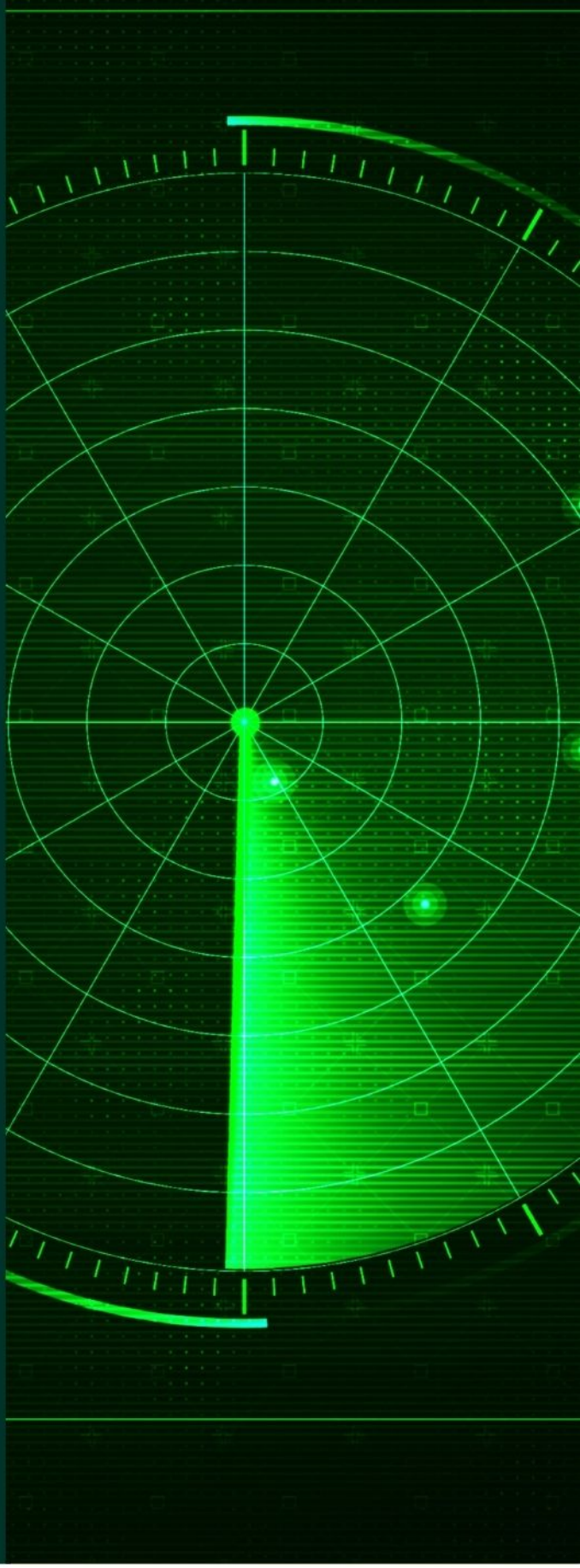

The Institution of Engineering and Technology

Received: 15 May 2023 | Revised: 5 September 2023 | Accepted: 8 September 2023

IET Radar, Sonar & Navigation

DOI: 10.1049/rsn2.12475

ORIGINAL RESEARCH

Global Navigation Satellite Systems disciplined oscillator synchronisation of multistatic radar

Piers J. Beasley | **Nial Peters** | **Colin Horne** | **Matthew A. Ritchie**

Department of Electronic and Electrical Engineering, University College London, London, UK

Correspondence

Piers J. Beasley.
Email: piers.beasley.19@ucl.ac.uk

Funding information

Air Force Office of Scientific Research; Engineering and Physical Sciences Research Council; Defence and Security Accelerator; Defence Science and Technology Laboratory, Grant/Award Number: DSTLX-1000139871

Abstract

A fundamental challenge in the practical implementation of multistatic radar systems (MSRS) is the requirement for precise time and frequency synchronisation between the spatially separated radar nodes. The authors evaluate the performance of different classes of commercially available Global Navigation Satellite Systems (GNSS) timing receivers, Local Oscillators (LO) and GNSS Disciplined Oscillators (GNSSDOs) to determine the limitations of using one-way GNSS Time and Frequency Transfer (TFT) in this application. From evaluating the performance of three pairs of GNSSDOs, it is concluded that one-way GNSS TFT will likely be suitable only for the synchronisation of fully spatially coherent MSRS with carrier frequencies up to 100 MHz and waveform bandwidths up to 20 MHz. Whereas, in the case of short-term spatially coherent MSRS, synchronisation of systems with carrier frequencies up to a few GHz and waveform bandwidths of over 100 MHz will likely be possible. The performance of the different classes of GNSSDOs during GNSS denial (holdover) are evaluated, where it is concluded that frequency offsets between LOs at the point of GNSS denial will often significantly contribute, or even dominate, the holdover performance. Analysis of two practical multistatic radar measurements verifies the function of using the GNSSDOs for wireless synchronisation of the ARESTOR MSRS.

KEYWORDS

distributed sensors, multistatic radar, oscillators, radar detection, sensor fusion

1 | INTRODUCTION

Unlike conventional monostatic radar, where the transmit and receive elements are co-located, multistatic radar is a class of radar that have multiple spatially distributed transmitter and receiver nodes. The raw data, detections or tracks from each receiver are then jointly processed at a central Fusion Centre (FC). Multistatic radar systems (MSRS) benefits are fundamentally derived from the spatial diversity of radar node locations. The extra channels of information obtained for the same target, but from different view angles can allow an improved level of sensitivity to be achieved in some configurations [1]. The probability of a target being obscured is also reduced in MSRS configurations and the diversity in view angle often means stealthy targets are observed from bistatic angles that result in higher Radar Cross Sections (RCS) than monostatic radars [2], improving the probability of detection. The performance improvement is dependent on the level of cooperation between nodes and the level of node-to-node synchronisation achievable [1, 3].

For permanent static deployments of MSRS, the use of physical synchronisation cables between nodes may be feasible in some applications. Typical time transfer accuracy capabilities of between 1 and 10 ns have been reported using co-axial cable [4], however signal dispersion/attenuation will considerably limit achievable baselines using this method. Longer baselines and higher accuracies have been reported for time transfer using fibre-optics [4–8]. White Rabbit (WR)— a fibre optic based precision time protocol (PTP) originally developed for the Large Hadron Collider project— has been shown to

provide sub-nanosecond synchronisation via fibre-optic links [9, 10]. In previous literature Lewis et al. investigate the use of the WR PTP for synchronisation of multistatic pulse-Doppler radar in Refs. [6–8].

For MSRS with portable, moving or widely spaced nodes the requirement for physical synchronisation cables is often impractical or prohibitively expensive. As such, in these scenarios wireless node-to-node synchronisation is required. In Ref. [11], the WR PTP has been implemented over the air using 71–76 GHz mm-wave carriers, where comparable sub-nanosecond timing accuracy was attained to the previous implementations that required fibre-optic links. In a recent work [12], the direct breakthrough between two Aveillant Gamekeeper staring radar was used for post-capture range and phase correction of the staring passive bistatic node. A challenge for these wireless direct synchronisation implementations is the requirement for uninterrupted line-of-sight between nodes, it is likely also that synchronisation accuracy will be heavily dependent on the Signal-to-Noise-Ratio (SNR) and multi-path interference of the node-to-node wireless links [13].

Global Navigation Satellite Systems (GNSS) provide near ubiquitous worldwide coverage. GNSS constellations are predominantly used for position and navigation purposes, however can additionally be exploited as a source of Time and Frequency Transfer (TFT). GNSS timing receivers provide very good long-term time accuracy and frequency stability, however exhibit poor short-term stability, often referred to as timing jitter. In order to improve the short-term stability of a GNSS based TFT system, GNSS timing receivers are usually used to discipline some form of Local Oscillator (LO). In this GNSS Disciplined Oscillator (GNSSDO) configuration, both the long-term stability of the GNSS timing receiver and the short-term stability of the LO can be attained. Nearly all manufactures of GNSSDOs use one-way single carrier L1 timing receivers that use the Global Positioning System (GPS) constellation, and thus refer to the devices instead as GPS Disciplined Oscillators (GPSDO) [14]. The National Institute of Standards and Technology evaluate the performance of a variety of GPSDOs in Refs. [14, 15] where a thorough investigation of the sources of time and frequency offsets between devices can be found.

The works published by Sandenbergh et al. provide key references for the design of a one-way GPSDO based system for synchronisation of pulse-Doppler multistatic radar [16–20]. A derivation of the requirements for synchronisation of the experimental NetRAD and NeXtRAD MSRS is presented in Ref. [16]. A further piece of work by Sandenbergh et al. presents the development of an adaptive two-way TFT system for distributed time, frequency and phase synchronisation of radar networks [21]. Preliminary time and frequency measurements of the system were conducted whilst connecting the system nodes via a 1.5 m lengths of coax cable, an approximate ± 1 ns time error and the peak fractional frequency offset (FFO) of $\pm 4 \times 10^{-10}$ were observed. In Ref. [22], a two-way time transfer method using satellite communications is presented, using this method sub-ns timing accuracies can be achieved in high SNR links. A disadvantage of such two-way TFT methods is the considerable increase in the cost and complexity of the system [4].

In a previous publication by the authors of this paper, the performance of two different models of commercial-off-the-shelf (COTS) GPSDOs are evaluated [23]. This paper is an extension of that work and provides further analysis of the performance of the constituent parts of the COTS GPSDOs. This paper additionally provides analysis of the performance enhancement attained by upgrading GPSDOs from single-frequency GPS timing receivers to use a multi-GNSS dual-frequency timing receivers. The main novel contributions of this work are as follows:

1. An analysis of the synchronisation requirements for different classes of MSRS. There is limited existing literature relating the MSRS information fusion level to the required time, frequency and phase synchronisation between nodes of the MSRS.
2. Empirical measurements of the relative synchronisation between three classes of COTS GNSSDO. Very little work is published detailing results for relative GNSSDO-to-GNSSDO time, frequency and phase synchronisation. Instead, most existing literature and GNSSDO data sheets relate long-term GNSSDO synchronisation to absolute Coordinated Universal Time (UTC), which is of limited interest in context of MSRS synchronisation.
3. Analysis of GNSS denied performance for different GNSSDO technologies. A review of the holdover performance of two different LO technologies and estimations of MSRS performance when operating in GNSS denied scenarios.
4. Analysis of practical MSRS measurements captured during field trials. Comparison of practical MSRS performance whilst disciplined to GPS, and a second measurement whilst operating in a GPS denied scenario.

The remainder of this paper is organised as follows: an overview of the synchronisation requirements for different classes MSRS is provided in section 2. Analysis of the performance of different classes of commercially available GNSS timing receivers, LOs, and GNSSDOs is presented in section 3. Section 4 describes development and calibration of the RadSync GNSSDO based MSRS synchronisation system. In section 5, operation of the ARESTOR radar system in a multistatic configuration is described and two practical radar measurements are analysed. Finally, the conclusions of this work are summarised in section 6.

2 | MULTISTATIC RADAR SYNCHRONISATION

In most conventional monostatic radar systems a single Master Oscillator (MO) is used as a reference to derive to system-wide time, phase and frequency [7]. High quality ovenised crystal oscillators (OCXO) are most commonly used as this primary reference, from which a Stable Local Oscillator (STALO) is

derived. This STALO is then used for clocking digital circuitry, for example, Analogue-to-Digital Converters (ADC), and for deriving the pass-band LO for up- and down-conversion in heterodyne architectures. In monostatic radar there is rarely a requirement for an accurate absolute time or frequency reference, as all trigger and control signals will be relative to a common local reference, provided by the STALO [7]. The primary concern in monostatic systems is the phase noise performance of the STALO as this will limit the performance of even the most advanced of today's radar systems [24]. The phase noise of the STALO is a product of both the MO phase noise itself and the additive phase noise from derivative clock frequency circuits such as Phase Locked Loops (PLLs) [25, 26]. In MSRS transmitters and receivers are spatially separated, usually at distances that prohibit STALO distribution using direct methods such as physical clock distribution cables. This presents a considerable challenge in the practical implementation of such systems. Local STALO generation is almost always required at each node of the system. If no TFT method is implemented these individual STALOs will diverge in time and frequency, even if initially synchronised before deployment. Divergence in time and frequency between these distributed STALOs will lead to proportional range estimation and Doppler velocity estimation errors, considerably hindering the performance and subsequent use of the MSRS.

2.1 | Classes of multistatic radar systems

There are several factors that determine the time and frequency synchronisation requirement between the independent STALOs in MSRS, however in-general the requirements are dependent on the class of the MSRS. In Ref. [3], Chernyak proposes MSRS can be split into three classes depending on the spatial coherence of the system, namely, '*fully spatially coherent*', '*short-term spatially coherent*' and '*spatially non-coherent*'. An important attribute for differentiating between classes of MSRS is the degree of autonomy of signal reception [1, 3]. In MSRS with independent signal reception, individual nodes only receive signals emitted by their own dedicated transmitters. Multistatic radar systems of this type can be considered as a network of monostatic radars and thus are typically referred to as netted radar. Netted radars of this type often only require temporal coherence and thus fit into the class of spatially non-coherent radars, such systems are limited to incoherent radar data fusion methods. In Ref. [1], Hume et al. describe some of the benefits available to such networks of monostatic radars. In MSRS with cooperative signal reception, radar nodes can receive and process target echoes resulting from transmissions from other radar nodes, in addition to their own emissions. There are some considerable benefits of cooperative signal reception. One being, some nodes of the system can operate as purely passive receivers, allowing them to remain covert and undetectable to non-cooperative Electronic Support Measures. Multistatic radar systems with multiple receivers and transmitters will also offer graceful degradation if the systems comprises of several transmit and receive nodes. Multistatic radar systems with cooperative signal reception require a minimum short-time spatial coherence, however as found in Ref. [1] the best performance enhancement will be enjoyed by fully spatially coherent MSRS. In Ref. [1], Hume et al. derive an equation to quantify the sensitivity improvement of systems with cooperative signal reception. The system sensitivity was found to be a function of the square of the number of nodes, N^2, for coherent operation. Whereas, in the non-coherent case the sensitivity improvement results in an N fold improvement only.

The level that the radar data are jointly processed at the FC, dictates the MSRS coherence required. Multistatic radar systems fusion strategies are commonly split in to two classes, centralised and decentralised, dependent on the level of the radar data that are shared for joint processing in the FC. In centralised fusion strategies all signals, noise and interference from the spatially separated nodes are jointly processed at the FC. As found in Ref. [1, 3, 27] coherent centralised fusion techniques will provide the highest sensitivity improvement under certain scenarios, however this requires a fully coherent MSRS, where long-term node-to-node phase synchronisation is required [3, 27]. The requirement for fully coherent MSRS makes coherent centralised fusion the most complex and costly strategy to implement. The need for phase synchronisation can be relaxed if incoherent methods of data fusion are used, where only short-term spatial coherence is required [3]. In the second class of decentralised fusion strategies, thresholding and parameter estimation are conducted locally at each radar node before plots or tracks are jointly processed at the FC. In Ref. [3], Chernyak finds that the loss of information resulting from local thresholding results in an equivalent MSRS sensitivity loss which increases with the number of nodes in the system, making decentralised strategies sub-optimal. However, the requirement for high-bandwidth data-links between nodes makes implementing centralised fusion strategies difficult in practice, therefore MSRS deployments with decentralised fusion methods are considerably more common [3].

The spatial coherence of the MSRS itself is not the only factor that determines the appropriate information fusion strategy, the relative position of nodes, terrain topology, target location and expected complexity of the target's fluctuations are also important. Multistatic radar systems deployments with inter-node separation on the order of a small fraction of expected target-to-receiver and target-to-transmitter ranges, generally observe targets from the same aspect angles, as such target fluctuations are usually mutually correlated between receivers [27]. Such system topologies are often associated with sparse arrays. For Swerling 1 targets, with comparably large sizes, compared to the radar's RF wavelength, target fluctuations are understood to de-correlate with increasing inter-node separations [3, 27]. However, fluctuations received from comparably small simple targets may well be highly correlated for any topology [27]. In Refs. [3, 27], further analysis can be found on the spatial coherence of target fluctuations in systems with a variety of multistatic topologies. One should note, that target returns from an isotropic point scatterer would be

mutually correlated for any MSRS topology [27]. To that end, when considering a MSRS synchronisation requirements one should first consider the expected spatial coherence of target fluctuations observed by each receiver.

2.2 | Time accuracy

Spatially non-coherent netted radar systems, with independent signal reception, usually share plot or track information [3], as a result these systems have the least stringent node-to-node time synchronisation requirements. That said, some degree of temporal coherence will still be required to permit plot or track association in the FC. In contrast, for MSRS with cooperative signal reception, a highly accurate common appreciation of time between the transmitter and receiver nodes is required for accurate bistatic range estimation [4]. Any time offset between a spatially separated transmitter and receiver nodes will result in a bistatic range estimation error, ΔR_b. The magnitude of this bistatic range error can be calculated by $\Delta R_b = \Delta t_b c$, where Δt_b is the time offset between nodes and c is the speed of light. Timing accuracy requirements in bistatic and MSRS are typically derived from the bandwidth, B, of transmitted waveform, where accuracies in the order of a fraction of the radars compressed pulse width are required [4, 7, 13, 20]. To give example, Equation (1) relates the timing accuracy, Δt_a, required to achieve an accuracy of one-10th of the compressed pulse width, τ_{pulse},

$$\Delta t_a = \frac{\tau_{pulse}}{10} = \frac{1}{10B} \tag{1}$$

Figure 1 plots the linear relationship detailed in Equation (1) between radar bandwidth and required timing accuracy. In summary, MSRSs with greater waveform bandwidths require higher accuracy node-to-node timing synchronisation.

2.3 | Frequency accuracy

Multistatic radar systems with cooperative signal reception, require node-to-node frequency synchronisation of STALOs to allow for carrier frequency, base-band sampling, and data clock synchronisation. Frequency offsets between STALOs will result in carrier frequency offsets, which in turn will result in Doppler estimation errors. A fixed deviation in carrier frequency, Δf_c, over the radars coherent processing interval (CPI) will result in a proportional Doppler estimation error equal to Δf_c. Should Δf_c vary during the period of the CPI, Doppler spreading will occur [20, 28]. Frequency offsets between STALOs scale to deviations in carrier frequency according to the following:

$$\Delta f_c = \frac{\Delta f_o}{f_o} \times f_c \tag{2}$$

where f_o is the STALO frequency, Δf_o is the offset in frequency between the two STALOs, and f_c is the radar carrier frequency. One can deduce from this that MSRS with higher carrier frequencies will be more susceptible to Doppler errors caused by STALO offsets. The equivalent velocity error is of course invariant of carrier frequency and can be calculated by multiplying the FFO between STALOs by c, which is given as follows:

$$\Delta V = \frac{\Delta f_o}{f_o} \times c \tag{3}$$

where ΔV is the Doppler velocity error, in ms^{-1}. Significant enough STALO frequency offsets will cause false transmitter and receiver velocity errors, which will impart a false Doppler shift on static targets and clutter [20], and may additionally interfere with Moving-Target-Indicator filtering used for suppression of static clutter [13]. In short-term spatially coherent radars, with cooperative signal reception, the Doppler velocity resolution, V_r, of the radar can be used to derive the required STALO frequency synchronisation (a radar's V_r is dependent on a mixture of radar's central frequency and signal processing parameters). The level of data fusion in MSRS FC will additionally determine the frequency synchronisation accuracy required. For decentralised fusion approaches, such as plot or track level fusion, Doppler velocity errors of less than the velocity resolution should suffice, in this case $\Delta f_c < V_r/c$ [7]. However, should a more complex centralised fusion approach be desirable, Doppler velocity errors of fraction of the V_r of the radar would likely be required.

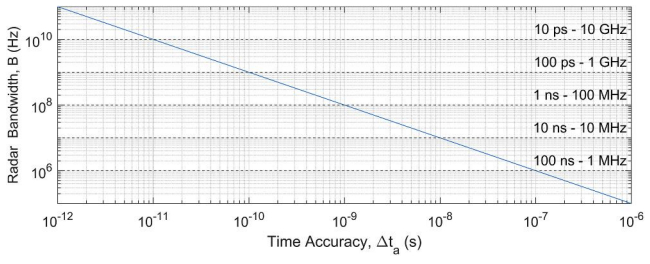

FIGURE 1 Timing accuracy requirements for the synchronisation of fully and short-term spatially coherent multistatic radar systems (MSRS) as a function of radar bandwidth.

2.4 | Long term phase stability

For cooperative signal reception in MSRS, the node-to-node phase stability requirements are identical to that of a monostatic system [20]. The required phase stability for independent STALOs is dependent on the duration and method of coherent processing [20]. Willis states in Ref. [13] that the required LO stability σ_y, over the CPI τ_{int} can be expressed as follows:

$$\sigma_y(\tau_{int}) = \frac{\Delta\phi}{2\pi f_c \tau_{int}} \tag{4}$$

where f_c is the radar carrier frequency and $\Delta\phi$ is the permissible phase offset over τ_{int}. One should note that (4) assumes no initial phase or frequency offset between the independent STALOs, which, as observed in the works by this author, and additionally commented on in Ref. [20], is not always a realistic assumption for indirectly synchronised STALOs.

In fully spatially coherent MSRS that employ coherent radio signal level fusion of the MSRS data, long-term node-to-node phase alignment of the carrier frequency must be maintained [3, 27]. Phase alignment in the order of a fraction of the radar's carrier frequency wavelength would be required for such systems [27]; this often far surpasses the aforementioned time accuracy requirements described in section 2.2. Figure 2 shows the equivalent phase time synchronisation requirements as a function of MSRS carrier frequency for a variety of permissible errors in carrier phase, $\Delta\phi$. For a MSRS with a f_c = 10 GHz phase time errors of less than 12.5 ps, 4.2 ps, 0.28 ps would be required for $\Delta\phi$ of 45°, 15° and 1°, respectively. In short term spatially coherent MSRS, the initial node-to-node phase shifts at the beginning of each CPI are random and mutually independent [3], as such the divergence in phase over the CPI is of primary concern.

2.5 | Short-term phase stability - phase noise

An important measure of radar performance is its Sub-Clutter Visibility (SCV), this defines the radar's dynamic range in the presence of a large clutter or target return [26]. The phase noise of a STALO reduces the ability of the radar to detect low RCS slow-moving targets in the presence of larger clutter returns [7, 20]. A radar's SCV is heavily dependent on the close to carrier, or close-in, STALO phase noise. This close-in region is dominated by noise sources that increase with decreasing frequency, for example, flicker noise [20]. Conventional monostatic radar systems, considerably benefit from using the same STALO for both up- and down-conversion, permitting significant cancelation random phase fluctuations and close-in phase noise of the STALO [7, 29]. In Ref. [29], Auterman found that systems that use independent STALOs for up- and down-conversion experience no cancelation of phase noise or spurious signals, instead the phase noise of the two STALOs adds up [20]. This lack of close-in phase noise cancelation, combined with the summation of phase noise, will considerably impact the SCV of MSRSs. It should be noted that the full phase noise spectrum is of concern, as even though radars usually have Pulse Repetition Frequencies (PRF) in the order of kHz, the STALO noise that extends beyond this range is aliased. This aliasing of higher frequency components back into the Doppler spectrum increases the Doppler spectrum noise floor [7]. In summary, if monostatic levels of SCV are required, STALOs with a great deal lower phase noise than typically used in monostatic radar are required [29].

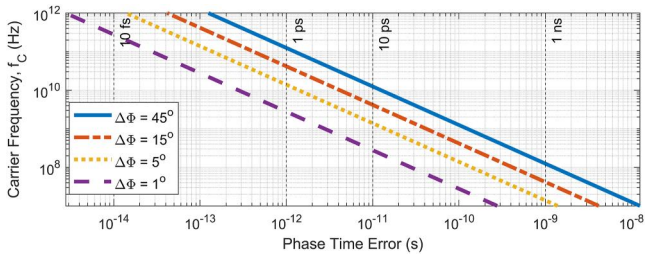

FIGURE 2 Required node-to-node phase time synchronisation, versus radar carrier frequency f_c, for a variety of permissible errors in carrier phase, $\Delta\phi$. Illustrating the stringent phase accuracy requirements for fully spatially coherent multistatic radar systems (MSRS).

3 | GNSS DISCIPLINED OSCILLATORS

In Sandenburg et al.'s works [16–20], bespoke quartz based GPSDOs were developed using low-cost COTS components in order to provide wireless synchronisation to the NetRAD and later NeXtRAD MSRSs. However, over the past decade there has been both an increase in the number of GNSS receivers and GNSSDO devices available on the consumer market and a reduction in their price. In this section, the performance of two classes of COTS GNSS timing receivers and two LO technologies will be investigated, before the performance of three models of COTS GNSSDOs are evaluated, namely: low-cost double-OCXO (DOCXO) based Trimble Thunderbolt E GPSDOs (THUN-E), Rubidium based Spectratime LNRCLOK-1500 GPSDOs with single frequency GPS receivers, and the same LNRCLOK-1500 GPSDOs instead with a dual-frequency multi-GNSS receivers.

3.1 | GNSS timing receivers

One of the most important constituent parts of a GNSSDO is the GNSS receiver. These devices receive and process signals from one or more constellations of GNSS satellites to provide an estimate of position, velocity and time. GNSS timing receivers are a sub-category of GNSS receivers specifically designed for precise timing synchronisation, in comparison to many other GNSS receivers designed for precise positional accuracy to aid in tasks such as navigation. In order to achieve the best timing performance, GNSS timing receivers should be configured to operate in a static mode, where the position of the receiver is assumed to be fixed. When the receiver is configured in this mode the accuracy of the positional estimate, calculated via multilateration, can be considerably improved through averaging many positional estimates, a process referred to as self-survey. After the self-survey has been completed the receiver uses fixed co-ordinates and only a timing fix is calculated. In this section, the relative timing performance of two different models of GNSS timing receivers are evaluated. The first model is the UBLOX LEA-6T GPS timing receiver, the second model is the more advanced UBLOX ZED-F9T multi-GNSS timing receiver. The LEA-6T receiver is a 50-channel single-frequency timing receiver that uses the L1 Course Acquisition code for the GPS constellation. Whereas the ZED-F9T is a 184-channel dual-frequency timing

receiver that has access to the US GPS, Russian GLONASS, European GALILEO, Japanese QZSS and Chinese BeiDou GNSS constellations. The ZED-F9T dual-frequency L1/L2 operation allows the device to compensate for ionospheric delays and therefore can considerably increase the timing accuracy without the need for any external GNSS correction service.

The relative timing performance of the UBLOX ZED-F9T and LEA-6T GNSS timing receivers were simultaneously measured over a period of 5 days. All four GNSS receivers shared the same L1/L2 GNSS antenna feed, split four-ways using a S14-GT-A GNSS signal splitter. The relative offsets between the one pulse-per-second (1PPS) timing outputs of each GNSS receiver was measured using a four-channel RTO2024 oscilloscope with a time resolution of 25 ps. Figure 3a shows a histogram of the relative performance of the two models of GNSS receivers; In this figure the mean time offsets have been removed. The offsets of both GNSS receivers appear to have a Gaussian distribution, where the F9T receivers provide a 2.5 times smaller standard deviation, 1σ, than the 6T receivers. The 25 ns peak-to-peak timing offsets between the F9T receivers were a factor of two smaller than the 6T receivers.

The most common time domain measure of frequency stability is the Allan Deviation (ADEV) [30], an overlapping version of the calculation is often now used to improve the confidence in the ADEV stability estimates, referred to as the Overlapping Allan Deviation (ODEV). Overlapping Allan Deviation evaluates the unit-less fraction frequency stability, σ_y, of a reference, as of function of averaging time, τ, in s. The four-channel RTO2024 oscilloscope ODEV accuracy was calibrated to find noise floor of $\sigma_y\ (1) = 1 \times 10^{-10}$ and $\sigma_y\ (100) = 1 \times 10^{-12}$, reducing with a constant -1 gradient with increasing averaging time. The relative frequency stability of the GNSS receivers outputs were analysed using the ODEV and can be found in Figure 3b. Both receivers slopes follow a -1 constant gradient which is indicative of either the white or flicker phase modulation noise. The modified ADEV was used to distinguish that the noise was in-fact white phase modulation (WPM) [30]. The F9T receivers were found to provide a 50% better frequency stability than the L6T receivers. In summary, if the raw GNSS receiver 1PPS outputs were used for time synchronisation, the two standard deviation, 2σ, accuracy (equivalent to the 95.4% confidence interval) would be limited to 6.82 and 17.36 ns for the F9T and 6T GNSS receivers, respectively, equivalent to bistatic range errors of 2.04 and 5.20 m. The measurement result statistics of the relative performance of the two models of GNSS receivers can be found in Table 1.

A considerable source of short-term instability, commonly referred to as timing jitter, results from the fact most GNSS receivers utilise low-cost free-running onboard oscillators that are not phase locked to UTC time. GNSS timing receivers can very accurately determine when the top of the second will occur, however in most cases the raw 1PPS timing output will be derived from the onboard oscillator. This means the 1 Hz signal cannot be perfectly reproduced, instead, the 1PPS signal is superimposed with a zero-mean saw-tooth quantisation error [20]. Therefore, receivers with higher frequency onboard oscillators provide a better time pulse resolution and are less adversely affected by saw-tooth error. Most GNSS receivers supply the user with

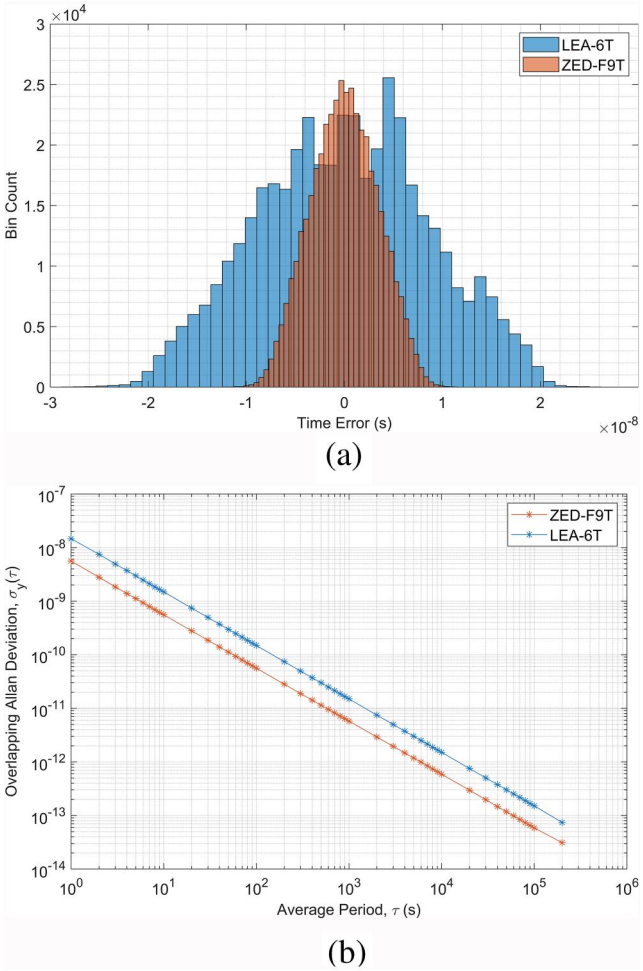

FIGURE 3 Relative 1PPS stability between pairs of UBLOX ZED-F9T and LEA-6T Global Navigation Satellite Systems (GNSS) timing receivers. (a) Histogram of time error between receivers. Mean time offsets were first removed. (b) Overlapping Allan Deviation (ODEV) detailing the relative 1PPS frequency stability between receivers as a function of averaging time.

TABLE 1 Relative timing error statistics for pairs of UBLOX ZED-F9T and LEA-6T Global Navigation Satellite Systems (GNSS) timing receivers and their equivalent bistatic range error.

GNSS receiver	LEA-6T	ZED-F9T
Mean (ns/m)	5.94/1.78	1.94/0.58
Pk-Pk (ns/m)	58.07/17.40	24.95/7.48
1σ (ns/m)	8.68/2.60	3.41/1.02
2σ (ns/m)	17.36/5.20	6.82/2.04
ODEV, $\tau = 1$s	1.45×10^{-8}	5.59×10^{-9}

the estimate of the quantisation error before outputting the 1PPS pulse, permitting the removal by the user in some later processing step. A considerable improvement in the timing accuracy of the GNSS receivers would be expected if a saw-tooth correction step was additionally implemented.

3.2 | Local Oscillators

In the previous section the relative synchronisation of two different GNSS timing receivers were analysed. Figure 3b shows the poor short-term stability of the two models of receiver, signified by the large deviations in frequency at small averaging times. However, the good long-term stability of the GNSS timing receivers is shown by the several orders of magnitude smaller deviations in frequency at long averaging times. In order to attain good short-term stability, GNSSDOs additionally contain a high stability LO.

Quartz crystal oscillators (XO) provide a low-cost frequency source that exhibit excellent short-term stability and are often unbeatable for the 1–100 MHz range for periods less than 1 s [31]. The greatest challenges of XOs is their temperature based frequency dependence and poor ageing rate. The impact of temperature variations can be overcome in a variety of ways, however if optimal stability is required XOs are encased in high-precision ovens to accurately control the temperature of the crystal, referred to as oven controlled crystal oscillator (OCXO). Even greater stability under temperature changes can be attained by encasing the XO in a double oven system, referred to as a DOCXO. Atomic frequency standards look to provide considerably improved long-term stability in variable environmental conditions. The stability and accuracy of the clock is determined by the intrinsic properties of the electronic and nuclear structure of the atom, unlike in crystal oscillators, where the stability is dependent of the bulk properties of the crystal [31]. In passive atomic frequency standards, such as Rubidium and Caesium, a XO is locked to the atomic transition frequency through some form of control loop [32]. The time constant of this control loop governs how quickly it can respond to errors and time constants of 1s or less are standard. For timescales less than the time constant the clocks instability is dictated by the instability of the XO, whereas for timescales longer than the time constant the instability is dominated by variations in the atomic resonance [32]. In this work the performance of a DOCXO, contained with the Trimble Thunderbolt E GPSDO, and Rubidium Lamp-Pumped atomic clock, contained within the Spectratime LNRCLOK-1500 GPSDO will be reviewed.

3.2.1 | LO short term stability - phase noise

For timescales of less than 1s, the short-term frequency stability of oscillators is typically quantified via spectral phase noise analysis. Phase noise measurements describe the power-spectral-density (PSD) of the phase fluctuations as a function of frequency. The most common function used to specify phase noise is the Single-Side-Band (SSB) phase noise [30]. The phase noise performance of each device will be a product of the quality of the 10 MHz quartz oscillator and clock buffer circuitry. Figure 4 shows the SSB phase noise spectrum for the 10 MHz output of the LNRCLOK-1500 and Thunderbolt-E GPSDOs. One should note, the LNRCLOK-1500 GPSDOs were purchased with the Ultra-Low-Phase noise option, which provides an improved phase noise and short term frequency stability performance in comparison to the standard model. An Anapico APH6040 phase noise analyser was used to measure each GPSDO output, where 10^4 cross-correlations were completed to reduce the noise floor of the measurements. One can observe the close in phase noise is dominated by flicker and white frequency modulation, indicated by the -2.5 gradient of the phase power slope. The close in phase noise (<10 Hz) is comparable between the two quartz oscillators, however the WPM noise floor is approximately 17–20 dB lower in the LNRCLOK-1500 devices. The LNRCLOK-1500's lower WPM noise floor will significantly reduce the noise floor of the radar Doppler spectra in the presence of strong clutter. Root Mean Squared (RMS) jitter is a common metric used for quantifying phase noise performance in the time domain [33]. In this the work the RMS jitter of each device was evaluated up to the measured offset of 1 MHz. The measured RMS jitter was found to be 134 fs and 750 fs for LNRCLOK-1500 and THUN-E devices, respectively.

3.2.2 | LO long term stability - frequency stability

In order to compare the frequency stability of the different LO technologies, relative stability measurements were conducted between pairs of co-located free running oscillators using a 5 port $K + K$ FXE phase and frequency measurement device. Figure 5a plots the ODEV for the relative stability of the free running oscillators. The short-medium term stability σ_y ($\tau < 200$) of the two LO technologies is comparable, where the LNRCLOK-1500 devices provide marginally better short-term performance. However, as expected, the long-term stability of the Rubidium based LNRCLOK-1500 devices considerably supersedes the DOCXO devices. In the context of GNSSDOs, using LOs with superior long-term stability may allow the GNSSDOs to

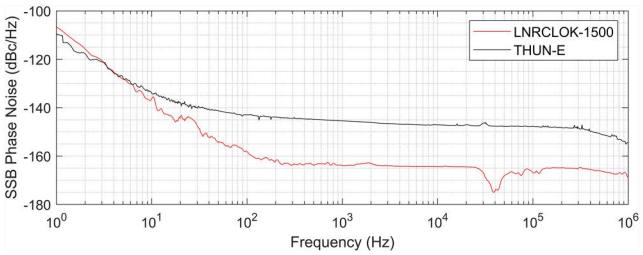

FIGURE 4 Single Side Band (SSB) phase noise of LNRCLOK-1500 and Thunderbolt-E 10 MHz outputs. Measured using APH6040 phase noise analyser with 10^4 correlations.

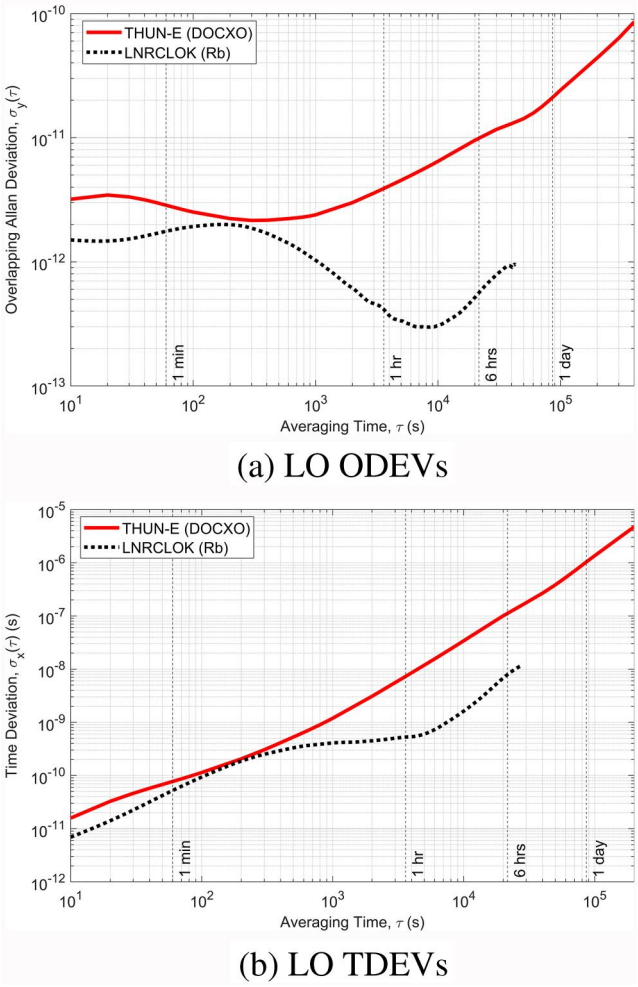

FIGURE 5 Relative stability between pairs of Thunderbolt E GPSDOs (THUN-E) and LNRCLOK-1500 free-running LOs. (a) Overlapping Allan Deviation (ODEV) comparing the relative frequency stability of the two LOs as a function of averging time; (b) Time Allan Deviation (TDEV) comparing the time deviation of LOs, as a function of holdover time, resulting from relative instability of the LOs.

stay synchronised for longer holdover durations in periods of GNSS outage. GNSS outages could be caused by interference, spoofing, signal jamming or constellation failure.

When analysing the ability of two LOs to remain time synchronised during periods of holdover the Time Allan Deviation (TDEV) is most commonly used [30, 32]. Time Allan Deviation, σ_x, allows predictions of time error to be analysed as a function of holdover time τ. Derivations of TDEV can be found in Refs. [30, 32]. One should note that time error between two LOs will not just be a function of the statistical fluctuations represented by TDEV, but instead also include contributions of initial time offset, T_0, frequency offset, $\frac{\Delta f}{f}$, long term frequency ageing, A, and integrated environmental errors, ϵ [32]. Time error, $\Delta T(\tau)$, over a holdover period, τ, can then be estimated using the following equation [32]:

$$\Delta T(\tau) = T_0 + \frac{\Delta f}{f}\tau + \frac{1}{2}A\tau^2 + \sigma_x(\tau) + \epsilon(\tau) \qquad (5)$$

However, for the purpose of this analysis, initial time offsets, frequency offsets, frequency ageing, and environmental errors will be treated as zero, leaving TDEV as the only factor contributing to time error in Equation (5). As stated in Ref. [32], it is can be assumed that ageing does not contribute to time error for the fairly limited holdover periods considered in this work. Figure 5b plots TDEV for the two LOs investigated in this work. Both LOs provide similar time deviations of <200 ps for holdover durations up to 200 s. However, after 15 min the time deviation of the DOCXO reaches 1 ns, whereas, the Rubidium LOs provide sub ns alignment for over 2 hours. Given TDEV does not account for any initial frequency offset, this estimate of time error is deemed to be very unrealistic when estimating the true holdover time deviation of the GNSSDOs technologies, further comment will be made in the following sections.

3.3 | COTS GNSS Disciplined Oscillators

The relative synchronisation of co-located GNSSDOs was measured in the lab. All devices shared a single GNSS antenna feed, split up-to four-ways using a S14GT-A GNSS signal splitter. Identical cable lengths were used where necessary. In the following sections the relative time and frequency synchronisation between three pairs of GNSSDOs is presented, namely: LNRCLOK-1500 GPSDOs with standard LEA-6T GPS timing receivers (LNRCLOK-L6T), LNRClok-1500 GNSSDOs with upgraded ZED-F9T timing receivers (LNRCLOK-F9T) and Trimble THUN-E.

3.3.1 | Relative timing accuracy

The relative timing accuracy between GNSSDO pairs was measured over a period of 6-days using the RTO2024 oscilloscope. All GNSSDOs were left to synchronise to UTC for a minimum of 2-days before measurements were started. The lab measured relative timing accuracy between the three GNSSDO pairings are plot in Figure 6 and the statistics for the three measurements can be found in Table 2. As expected all three GNSSDOs pairings exhibited a non-zero mean time offset. This static mean time offset between each GNSSDOs is a sum of the GNSS receiver self-survey error, fixed GNSS receiver 1PPS offset to UTC and internal GNSSDO delays [14, 17]. The self-survey error of the LNRCLOCK-F9T GNSSDOs should be smaller than the other models as the LNRCLOCK-F9T, as these models use differential GNSS timing receivers [34] and thus can more precisely determine the location of the GNSS antenna, as shown in section 3.1. Surprisingly, the LNRCLOCK-L6T pairing was found to provide the best relative timing precision, with a 1.65 ns mean offset between devices, though, considerably larger offsets of up to 10 ns have been observed in previous measurements of the LNRCLOCK-L6T GPSDOs. The THUN-E pairing provided the best timing accuracy with a two-sigma of 4.24 ns, equal to a bistatic range

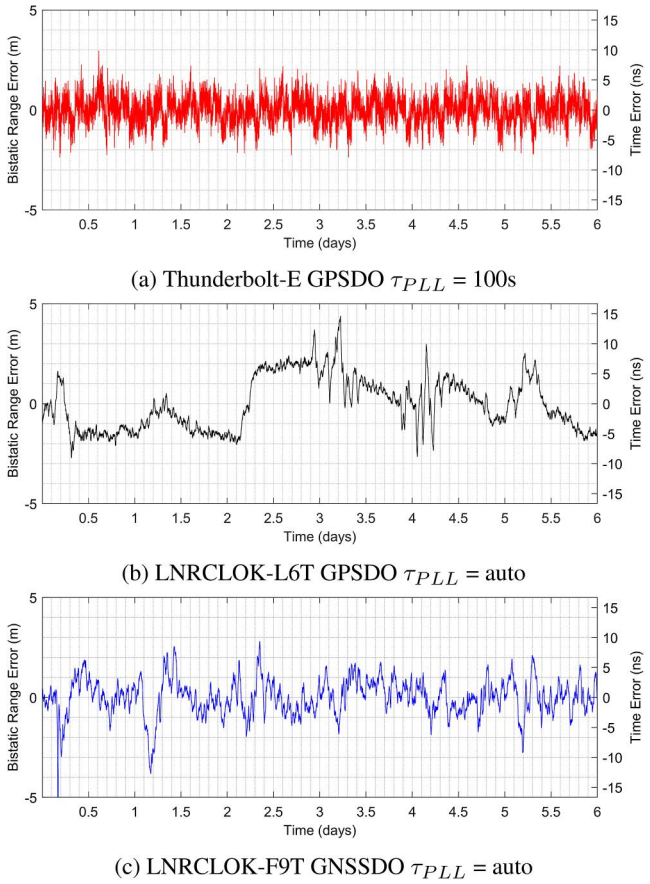

FIGURE 6 Plot of relative 1PPS timing errors between co-located GNSS Disciplined Oscillators (GNSSDOs) for a 6-day period. Mean timing offsets have been removed to ease comparison of relative timing performance. (a) Trimble Thunderbolt E (b) LNRCLOK-1500 with standard LEA-6T Global Positioning System (GPS) Timing Receiver (c) LNR-Clok-1500 with upgraded ZED-F9T timing receiver.

TABLE 2 Relative timing error statistics for three GNSS Disciplined Oscillator (GNSSDO) pairings and their equivalent bistatic range error.

GNSSDO model	THUN-E	THUN-E	LNR-L6T	LNR-F9T
τ_{PLL}	100s	1000s	Auto	Auto
Mean (ns/m)	16.52/4.95	2.57/0.77	1.65/0.49	2.19/0.68
1σ (ns/m)	2.12/0.64	2.19/0.66	4.42/1.32	3.06/0.92
2σ (ns/m)	4.24/1.28	4.28/1.28	8.84/2.64	6.12/1.83
Pk-Pk (ns/m)	17.80/5.33	16.50/4.95	23.70/7.10	35.63/10.68

error of 1.28 m. The LNRCLOCK-F9T provided the second best timing accuracy with a two-sigma of 6.12 ns, equal to a bistatic range error of 1.83 m. It should be noted, these measurements likely provide a best case scenario, the use of separate GNSS antennas over large bistatic baselines in environments with different ambient temperatures will likely deteriorate the relative timing performance to that measured in lab conditions [20, 23].

3.3.2 | Relative frequency stability

When the GNSSDOs are locked to GNSS, their internal disciplining circuity steers the stable internal LO towards the long-term average of the GNSS receiver's 1PPS timing output. The inner workings of the GNSSDO disciplining logic are rarely disclosed by manufactures, however the control loop is often some form of proportional-integral-derivative controller [14]. This control circuity measures the relative time error between the GNSS receiver output and LO output (usually after frequency division down to 1PPS). The control circuity then issues frequency corrections to the LO in order to align the phase of the LO to the long-term average of the GNSS timing receiver. In order to maximise the time and frequency synchronisation to UTC and thus between the GNSSDOs, the disciplining loop time constant, τ_{PLL} should be optimally tuned. This is done by comparing the stability of both the GNSS receiver 1PPS output with the stability of the internal LO. The time constant defines the point at which the GNSSDO adopts the stability of the GNSS timing receiver, before which, the stability is dependent on the internal LO [20]. The LNRCLOK-1500 GNSSDOs have an adaptive disciplining mechanism that dynamically adjusts the time constant by analysing the stability of the GNSS receiver's 1PPS signal against its highly stable internal Rubidium reference. The LNRCLOK-1500 device automatically adjusts the time constant. Time constants in the order of $3 - 6 \times 10^3$ s were observed when disciplining to the ZED-F9T GNSS timing receivers, whereas time constants on the order of 7–11 $\times 10^3$ s were observed when disciplined to the, less stable, LEA-6T GPS receivers. In contrast, the THUN-E GPSDOs have a static disciplining loop time constant and damping factor that can be adjusted by the user to alter the disciplining characteristics. The THUN-E time constant and damping factor are set to 100 s and 1, respectively, by the manufacturer.

The lab measured relative frequency stability of the GNSSDO pairs are provided as a function of averaging time in Figure 7. This figure includes the ODEV for LNRCLOK-L6T, LNRCLOK-F9T and THUN-E GNSSDO pairs. In the first THUN-E experiments, the disciplining loop characteristics were set to their manufacture defaults. One can observe the poorer short-to-medium-term stability, for σ_y ($\tau < 10^3$) of the THUN-E devices when compared to the Rubidium devices. To improve the short-to-medium stability of the THUN-E devices, the parameters of the disciplining loops were then optimised. This was achieved by comparing the stability of the internal LO to an estimated stability of the GPS receivers 1PPS (an estimate of the GPS receiver's stability had to be used, as there is no way to sample its output). An optimal time constant of ($\tau_{PLL} = 1000s$ was estimated [23]. The frequency stability of the THUN-E devices, with the optimised disciplining loop characteristics, is additionally plotted in Figure 7. A considerable improvement, of approximately a magnitude, in short-medium term relative frequency stability was attained. A marginal reduction in THUN-E timing performance was experienced, as tabulated in Table 2. The LNRCLOK-F9T was found to provide the best overall frequency stability.

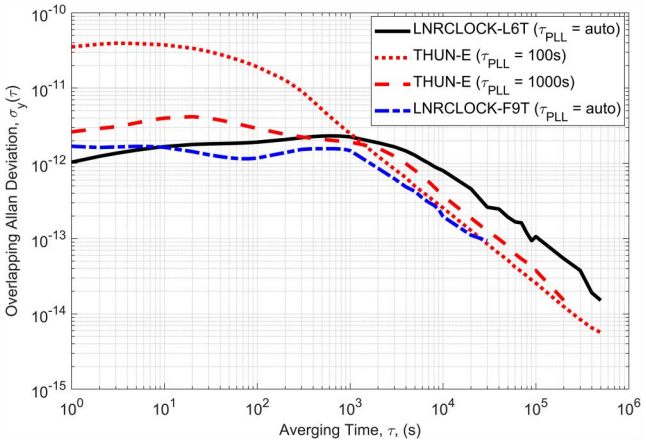

FIGURE 7 Overlapping Allan Deviation (ODEV) comparing the relative frequency stability of co-located GNSS Disciplined Oscillators (GNSSDOs) 10 MHz outputs versus averaging time, τ, whilst disciplined to Global Navigation Satellite Systems (GNSS).

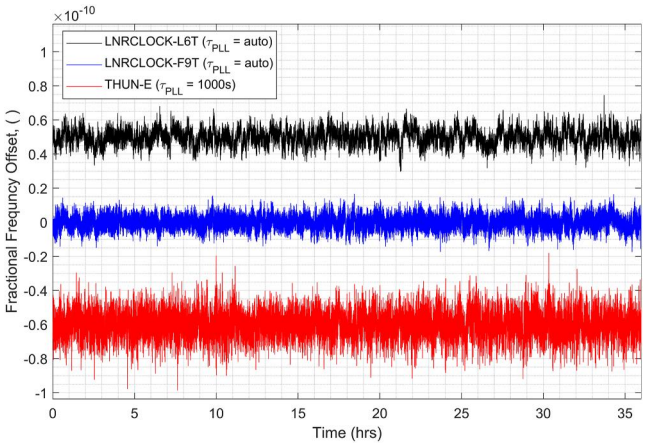

FIGURE 8 Relative fractional frequency offset (FFO), for $\tau = 1$s, between GNSS Disciplined Oscillator (GNSSDO) pairs for a 36-h period. Thunderbolt E GPSDOs (THUN-E) GPSDOs configured with adjusted disciplining loop parameters. Top plot of LNRCLOK-F9T data offset by 5×10^{-11}. Bottom plot of THUN-E data offset by -6×10^{-11}.

3.3.3 | Relative frequency accuracy

The relative FFO between GNSSDOs has been evaluated for 1 s averaging periods over a duration of 36-h. This allows the relative frequency errors between GNSSDOs to be evaluated for periods analogous to CPIs in radar signal processing. Figure 8 illustrates the FFOs for the three GNSSDO pairings over the 36-h measurement period. The statistics for measurements can additionally be found in Table 3, where the FFO statistics for the THUN-E, with sub-optimal disciplining loop time constants, have additionally been included. The LNRCLOK-F9T provide the best performance with both the lowest two-sigma and peak frequency offset. Using (2) and (3) the relative Doppler and velocity errors resulting from these LO offsets can be estimated. A 2.42 GHz radar carrier frequency is used to allow comparison with results presented later in this paper. The LNRCLOK-F9T peak offset would result in a 42 mHz Doppler error and a negligible 5.22×10^{-3} ms^{-1} Doppler velocity error. The THUN-E with $\tau_{PLL} = 1000$s provide similar frequency accuracy to the LNRCLOK-F9T devices with an approximately factor of two worse two-sigma and 2.5 times worse peak frequency error. The worst case frequency accuracy was measured for the THUN-E, with $\tau_{PLL} = 100$s, where a peak frequency offset two magnitudes worse than the LNRCLOK-F9T devices was observed, which would result in a considerable 3.30 Hz Doppler error and 0.41 ms^{-1} velocity error. The two-sigma frequency offset for the THUN-E with $\tau_{PLL} = 100$s, was approximately a magnitude less than their peak offset and thus would result in magnitude smaller Doppler and velocity estimation errors.

3.3.4 | GNSS Disciplined Oscillator holdover performance

In section 3.2.2 the ability of two LOs to remain time synchronised during periods of holdover was discussed. In that analysis when calculating $\Delta T(\tau)$ from (5), the FFO between oscillators was assumed to be zero to allow direct comparison of the time keeping stability of the oscillators, isolated from initial time and frequency synchronisation. However, from looking at the relative frequency offsets between GNSSDOs, whilst disciplined to GNSS, we have found the FFO between GNSSDOs are not zero. As such when GNSSDOs are forced into holdover, $\Delta T(\tau)$ will likely be dominated by the FFO in many scenarios. To provide example, in the case of the LNRCLOK-F9T, the TDEV of the LO was found to provide just 1 ns of time deviation for over 2 hours. Though, the ΔT resulting from relative frequency offsets between LNRCLOK-F9T GNSSDOs, as measured in section 3.3.3, would result in of 1 ns error in just 275 s (under 5 min), assuming the one-sigma value. Somewhat reducing utility in the more stable Rubidium frequency reference. That said, the LNRCLOK-1500 GNSSDOs did generally provide better relative frequency accuracy, thus the divergence in time will likely be lower than the THUN-E devices. The ΔT resulting solely from the two-sigma FFO values in Table 3 would result in ΔT of 629 ns, 801 ns, and 1.23 µs for 1-day of holdover for the LNRCLOK-F9T, LNRCLOK-L6T, and THUN-E GNSSDOs, respectively.

TABLE 3 Statistics of FFOs between GNSS Disciplined Oscillators (GNSSDOs), for a 1s averaging time, over a 36-h period.

GNSSDO model	THUN-E	THUN-E	LNR-L6T	LNR-F9T
τ_{PLL}	100s	1000s	Auto	Auto
1σ (10^{-12})	60.64	7.14	4.64	3.64
2σ (10^{-12})	121.13	14.28	9.27	7.28
Max (10^{-11})	136.41	4.20	2.47	1.74

4 | RADSYNC SYNCHRONISATION SYSTEM

In order to utilise the GNSSDOs for synchronisation of spatially separated radar nodes the RadSync multistatic radar synchronisation system has been developed at University College London. The RadSync system is used to derive the required synchronisation signals from COTS GNSSDOs, for three radar systems, namely, the bladeRAD hybrid radar system [35, 36], the ARESTOR multi-role RF system [37, 38] and the NeXtRAD multistatic radar system [39, 40]. The radar synchronisation system provides three main elements of functionality: synchronous clock signal conversion synchronous trigger generation and network control of the spatially separated synchronisation nodes. Figure 9 shows the main constituent parts of each synchronisation node and Figure 10 is a photograph of a single node of the system. Small single-board Raspberry Pi (RPI) computers are used for control of each node and connected over a Wireless Local Area Network. A custom interface card was designed for the frequency conversion and synchronous trigger derivation, all functionality of the circuits are controlled via the RPI.

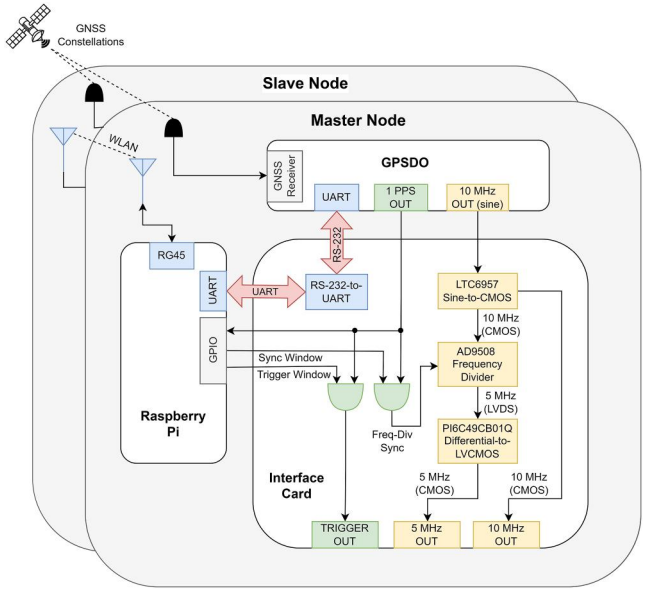

FIGURE 9 Diagram showing main constituent parts of GNSS Disciplined Oscillator (GNSSDO) based synchronisation system. Identical hardware setups are used at each radar node, control of the system is administered via Wireless Local Area Network (WLAN).

4.1 | Time synchronisation

In order to synchronise the acquisitions of multiple radar nodes a low-jitter trigger signal was derived from the 1PPS output of the GNSSDOs. To minimise the jitter of the trigger signal a hardware design was implemented. This solution results in a trigger accuracy that is only constrained by the degree of error between GNSSDOs 1PPS outputs, plus some additional skew introduced by the hardware trigger circuitry. The skew introduced by the trigger derivation circuitry was measured to have a mean of less than 0.15 ns, with a standard deviation of 12.1 ps, negligible in comparison to the measured 1PPS errors between co-located GPSDOs presented in section 3.3.1. Figure 11 illustrates a timing diagram showing the derivation of the radar trigger from the GNSSDOs 1PPS signals.

FIGURE 10 Photograph of a single node of the RadSync GNSS Disciplined Oscillator (GNSSDO) based multistatic radar synchronisation system. Raspberry Pi (RPI) single board PC (far left); Custom interface card (centre). Uninterruptible-Power-Supply (UPS) (far right). LNRCLOK GPS Disciplined Oscillators (GPSDO) visible in top right and Thunderbolt E GPSDOs (THUN-E) GPSDO visible top left.

4.2 | Clock synchronisation

The GNSSDOs stable 10 MHz clock outputs can be used to synchronise the STALOs in the spatially separated radar nodes.

4.2.1 | NeXtRAD

The NeXtRAD radar's frequency distribution unit will directly accept the 10 MHz sinusoidal output of the GNSSDOs [7].

4.2.2 | bladeRAD

The PLLs of the bladeRAD system requires a higher slew-rate 10 MHz 3.3 V complementary metal-oxide semiconductor

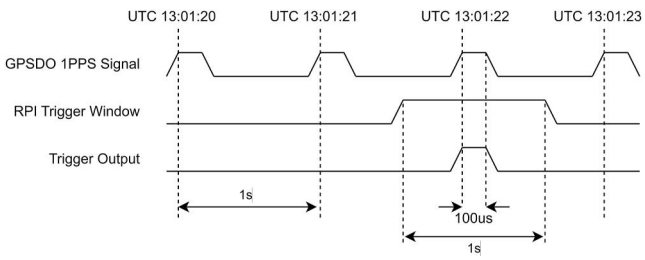

FIGURE 11 Timing diagram showing derivation of synchronous trigger signal from GNSS Disciplined Oscillator (GNSSDO) 1PPS signal.

(CMOS) clock signal. An LTC6957 low phase noise clock driver was used for conversion from sine-to-CMOS and output on an appropriate connector to supply the bladeRAD radar system.

4.2.3 | ARESTOR

The ARESTOR system requires a 5 MHz 3.3V CMOS signal. To synthesise the 5 MHz clock signal for the ARESTOR radar, from the 10 MHz GNSSDO references, a low-jitter AD9508 clock buffer was used for frequency division down from to 5 MHz. This device was selected for its low additive phase noise specification and ability to synchronise the edge on the output clock to the edge of the input clock. Synchronisation of clock edges across synchronisation nodes is required to ensure a common edge of the 10 MHz input is used for generation of the 5 MHz across multiple nodes. Should the 5 MHz synchronisation not occur, ARESTOR radar nodes may end up synchronised with a 100 ns (1 period of the 10 MHz) timing error between nodes, resulting in a considerable 30 m bistatic range error. Figure 9 illustrates the 5 MHz clock derivation showing how a common trigger is supplied to the frequency dividers at each synchronisation node. The output of the frequency divider is further converted from a Low-Voltage-Differential-Signal (LVDS) to a 3.3 V CMOS signal.

To evaluate the impact of the clock conversion and frequency division on the phase noise performance of the output clock signals, the phase noise of the 10 and 5 MHz CMOS clock outputs were measured. Figure 12 illustrates the SSB phase noise of the 10 MHz of the LNRCLOK-1500, input to interface cards, and the 5 and 10 MHz CMOS clock outputs of the synchronisation system's interface cards. The RMS jitter of each clock signal was evaluated up to a 1 MHz offset. The RMS jitter of the LNRCLOK-1500 input to the system was 137 fs, the CMOS conversion degraded the RMS jitter to 287 fs and conversion to 5 MHz further degraded the phase noise performance to 487 fs.

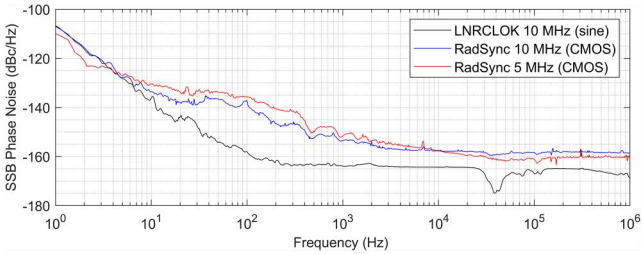

FIGURE 12 Single Side Band (SSB) phase noise of the RadSync clock outputs versus the LNRCLOK-1500 master LO 10 MHz phase noise. Measured using APH6040 phase noise analyser with 10^4 correlations.

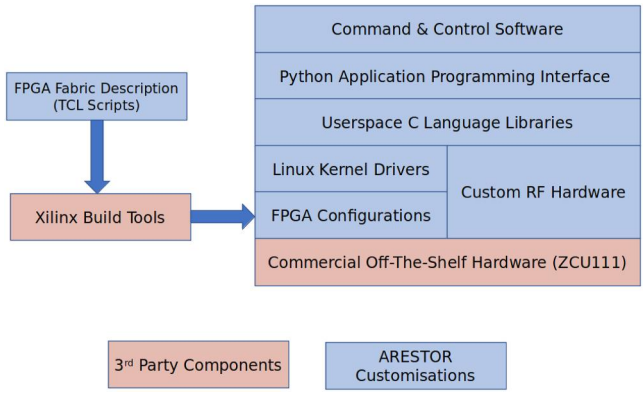

FIGURE 13 Block diagram showing the main components making up the ARESTOR system.

5 | ARESTOR MULTISTATIC RADAR SYSTEM SYNCHRONISATION

5.1 | ARESTOR radar system

The ARESTOR system [41] was developed at University College London (UCL) and is based on a Radio Frequency System on Chip (RFSoC) that was created by AMD-Xilinx. The RFSoC represents a tightly integrated Field Programmable Gate Array (FPGA), Arm processor and ADC/Digital-to-Analogue Converters (DAC) configuration that allows for a wide variety of applications including communications, radar and Electronic Warfare. As illustrated in Figure 13 ARESTOR uses the ZCU111 RFSoC evaluation board as its fundamental building block, and created a suite of custom hardware (e.g. Figure 14), software and FPGA configurations for it which enable transmit and receive on multiple channels, across different frequency bands, in a multistatic arrangement that can also use different sensing modes (Active Radar [42]/Passive Radar [37]/Joint Radar-comms. [43]). The different sensing modes can either be operated simultaneously (given sufficient FPGA resources for the required designs) or switched between in a matter of seconds. ARESTOR represents an almost unique combination of cutting edge tightly integrated digital hardware and firmware that has created an enabling piece of equipment for multiple research domains in the RF sensing field.

5.2 | ARESTOR multistatic synchronisation

The RFSoC device is structured such that its ADCs and DACs are grouped onto tiles. There are four tiles with 2 ADCs and 2 tiles with 4 DACs each on the RFSoC on the ZCU111 (which is a first-generation device); note that further generations of the hardware have different configurations. Within a given tile there is a PLL that is used to generate the sampling clock for all the DACs and ADCs linked to it. In order to use the full 8 channels for coherent RF sensing it is important to utilise the "multi-tile synchronisation" (MTS) capabilities that Xilinx has provided. MTS synchronises the PLLs that are on separate tiles as well as ensuring matched latencies as data are passed off of the tile and into the FPGA fabric. The MTS capability requires two coherent copies of a low frequency clock signal (called SYSREF) to be input to

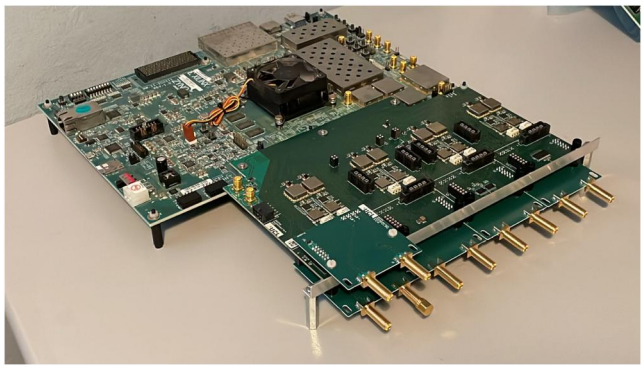

FIGURE 14 Photograph of the Radio Frequency System on Chip (RFSoC) (ZCU111) with the University College London (UCL) custom built daughterboard, which allows access to all 8 Digital-to-Analogue Converters (DACs) and Analogue-to-Digital Converters (ADCs) [38].

the RFSoC device. In order to synchronise multiple RFSoC devices (as is the case for a multistatic system), each device must receive coherent copies of these SYSREF clocks. A limitation of the ZCU111 is that these SYSREF clocks cannot be supplied externally, making multistatic deployments a challenge. However, the UCL system has been able to overcome this limitation and multiple ARESTOR nodes can be synchronised using MTS. The method used is described in detail within [38].

For the purpose of this publication ARESTOR was used as an active radar that was clocked using external GNSSDO based sources to provide real radar data that is dependent on the quality of the input clock phase noise, frequency stability and timing stability.

5.2.1 | Phase drift

In order to investigate how the phase error between independent STALOs propagates to ARESTOR radar carrier frequency phase error, a series of lab experiments were conducted. The ARESTOR radar was setup with a 2.42 GHz carrier frequency and used a frequency modulated continuous wave (FMCW) sensing mode with a pulse repetition frequency (PRF) of 1 kHz. In these experiments two ARESTOR nodes were used, each disciplined to separate RadSync GNSSDO nodes. One ARESTOR node's transmissions were split and then looped back to itself and also to the second bistatic node. This was done to simulate a static target at a known fixed range to allow the monostatic and bistatic carrier phase stability to be analysed whilst disciplined to GNSSDOs. The relative phase between two RadSync GNSSDO derived 5 MHz clock signals, used to clock the individual ARESTOR nodes, was logged at a 1 Hz rate using the RTO2024 oscilloscope. This relative LO phase error could then be compared to the radar phase error, measured using the radar. In order to determine the relative node-to-node carrier phase, the range bin containing the pseudo target was first identified. After which, the phase

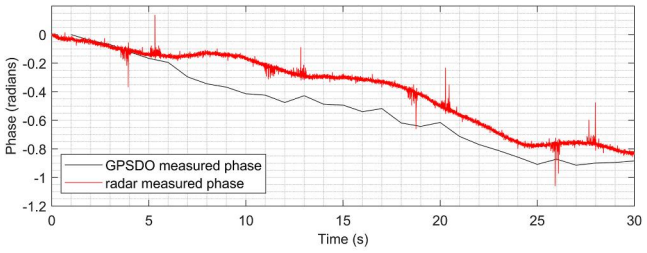

(a) Phase Series 1

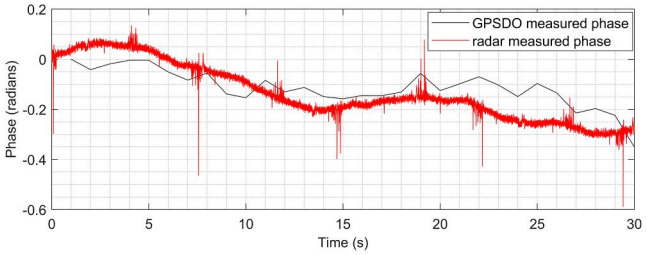

(b) Phase Series 2

FIGURE 15 Comparative plots of bistatic radar carrier frequency phase and independent LO phase for two 30s ARESTOR loop-back experiments. Showing clear correlation between independent LO phase error and radar phase error.

series was attained by taking the argument of the complex samples down the slow-time dimension of the radar matrix. Figure 15 shows the relative carrier phase of the radar for two identical 30 s experiments. The relative phase between two RadSync GNSSDO derived 5 MHz clock signals was simultaneously sampled for the duration of the measurements. The relative 5 MHz LO phase was scaled to 2.42 GHz in order to allow direct comparison of the two phase series and plot alongside the radar phase. In both 30 s measurements there appears to be clear correlation between relative drift in RadSync LO phase and radar carrier frequency phase, confirming the lock of phase between RadSync LO and radar carrier frequency. This result does not confirm carrier phase synchronisation, but instead carrier phase coherence, that is, radar carrier frequencies are coherent, but may have a random fixed offset. The cause of the periodic high-frequency phase excursions in the radar phase data is not yet known.

5.2.2 | Phase noise

The phase noise of the ARESTOR 5 MHz STALO was measured both whilst disciplined to the low phase noise LNRCLOK MO, and whilst free running using its onboard Si570 XO as a MO reference. SSB phase noise spectrum plots can be found in Figure 16 for these measurements. When disciplined to the LNRCLOK MO, the ARESTOR STALO stability tends towards the stability of the MO for offset frequencies less than 30 Hz, after which the ARESTOR LMK04208 PLL VCO phase noise dominates. In this configuration the STALO takes advantage of the low close-in phase noise of the LNRCLOK MO. This

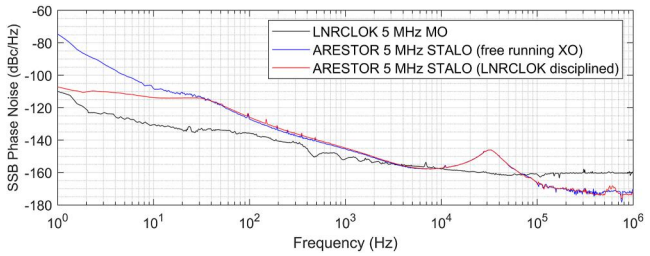

FIGURE 16 Single Side Band (SSB) phase noise of ARESTOR 5 MHz Stable Local Oscillator (STALO) whilst disciplined to low-phase noise LNRCLOK Master Oscillator (MO) versus onboard Si570 XO. Measured using APH6040 phase noise analyser with 10^4 correlations.

improvement in close-in phase noise will provide a significant improvement in the bistatic SCV of the radar, as described in section 2.5. The RMS jitter (evaluated up to a 1 MHz offset) of the ARESTOR STALO whilst free running using the onboard XO was measured to be 6.1 ps, reducing considerably to 797 fs when disciplined to the low-phase noise LNRCLOK 1500 MO reference. Further reduction in the ARESTOR STALO phase noise could be made by adjusting the LMK04208 PLL bandwidth to incorporate the lower LNRCLOK MO noise out to offsets of 7 kHz. This further reduction in STALO phase noise will further reduce the noise floor of the radar's Doppler spectra in the presence of strong clutter [7, 26].

5.3 | Multistatic experiment

A series of two node multistatic radar measurements were conducted to investigate the synchronisation of the ARESTOR system whilst disciplined to the Radsync synchronisation system. The ARESTOR system was configured in an S-Band FMCW mode with an 80 MHz bandwidth linear-frequency-modulated waveform. Both ARESTOR nodes were configured as transceivers; transmissions from each node were interleaved and both nodes digitised reflections from their own transmissions and transmissions from the second node. An overall PRF of 2 kHz was used, each receive channel had an equivalent PRF of 1 kHZ due the interleaved transmissions. LNRCLOK-L6T GPSDOs were used as the time and frequency references at each node, and were setup disciplined to GPS during the experiments.

A 50 m baseline was used between the two radar nodes. A static target was placed approximately 50 m from each radar node, such that an equilateral bistatic triangle was formed with the two radar nodes and the target. Figure 17 illustrates the experimental configuration. Wi-Fi point-to-point links were used for network control of the secondary node from the master node location. Figure 18 is a photo of the RadSync and ARESTOR ruggedised enclosures. Identical setups were used at each node for the experiments.

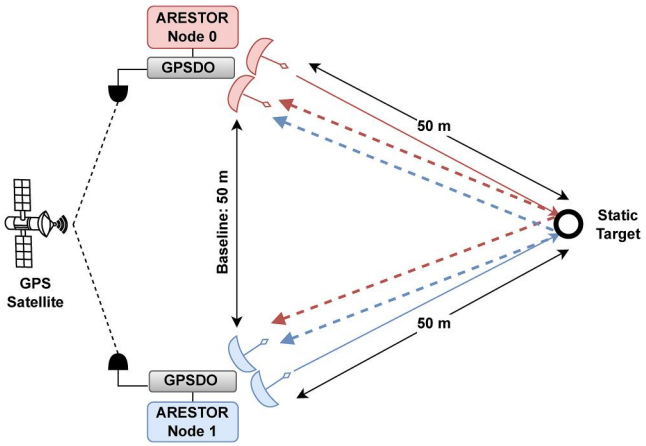

FIGURE 17 ARESTOR multistatic radar experimental configuration. Transmissions were made interleaved from each node.

FIGURE 18 Photograph of a single node of the multistatic radar system. ARESTOR multi-functional RF system node in bottom 4U rack. RadSync Global Positioning System (GPS) Disciplined Oscillator Synchronisation System node in 2U rack above.

5.3.1 | Global Positioning System synchronised measurement

Long-duration 900 s measurements were made of the static target in order to analyse the relative synchronisation between the two radar nodes. The first measurement was completed whilst disciplined to GPS. Figure 19a shows the range-time-intensity (RTI) plot of the bistatic reception of transmissions from ARESTOR node 0 to ARESTOR node 1. The radar measured range and true range of the target are plot in red and dashed red lines, respectively. A fixed bistatic range error of 10 m was observed during the measurement, equivalent to a time error of 33 ns between the independent GPSDOs synchronising each ARESTOR node. This considerable time error between nodes results from the GPSDOs being powered on within an hour of the radar measurements. It has been found

that GNSSDOs with long disciplining loop time constants can take several hours to reach optimal synchronisation to GNSS. As a result, in this interim period considerable time and frequency offsets are observed to be not in alignment with the results detailed in section 3.3. In order to analyse the relative phase stability between the two radar nodes, the unwrapped phase series of the static target are plotted in Figure 19b for both the bistatic and monostatic measurement. The disciplining characteristics of the GPSDOs can be observed in this plot, as the phase error between radar carrier frequencies oscillates around zero radians. A phase excursion occurs at 640 s, resulting from a considerable frequency offset developing between GPSDOs. The fractional frequency error between the two radar nodes was calculated from the phase data for a 1 s averaging time to allow direct comparison with the results in section 3.3.3. Figure 19c shows the fractional frequency error between radar nodes on the left axis and equivalent Doppler error, for the 2.42 GHz carrier frequency, on the right axis. The aforementioned frequency offset, developing at 640 s, is clearly observable in Figure 19c, and peaks at 3.07×10^{-11}, equivalent to Doppler and velocity errors of 74.3 mHz and of $9.2 \times 10^{-3}\ ms^{-1}$, respectively. The maximum FFO recorded in this measurement is over three times greater than the two-sigma FFO measured between the LNRCLOK-L6T GPSDOs in the lab measurements in section 3.3.3. The 33 ns time error also exceeds the maximum time error observed between the LNRCLOK-L6T GPSDOs in section 3.3.1 by 10 ns. If the GPSDOs had been left to reach optimal synchronisation to GPS a considerable improvement relative synchronisation performance would be expected.

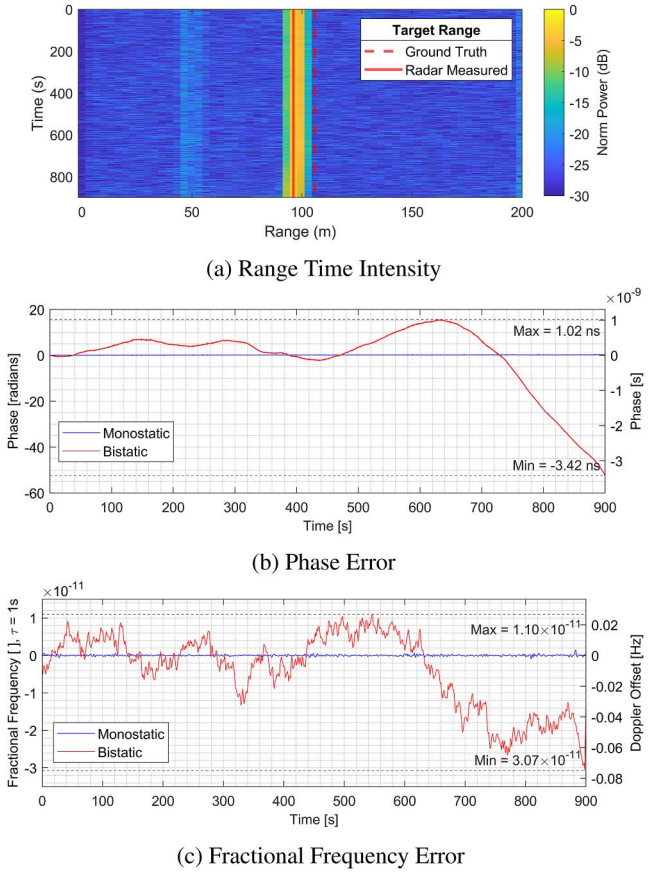

FIGURE 19 900 s measurement of a static target for long-term synchronisation analysis of the ARESTOR radar whilst disciplined to Global Positioning System (GPS) via the LNRCLOK-L6T GPSDOs. (a) Bistatic range time intensity plot. (b) Carrier phase of static target for monostatic and bistatic measurements. (c) Fractional Frequency error of carrier frequency for monostatic and bistatic measurements; low pass filtered and decimated to 1 Hz averaging period.

5.3.2 | Global Positioning System denied measurement - holdover

An additional 900 s radar measurement was conducted for the ARESTOR system during GPS denial, simulated via removing GPS antenna connections from the GPSDOs. This measurement started after approximately 15-min of GPS denial. GPS was denied for the entirety of the measurement. Figure 20a shows the RTI plot for the measurement, the static target starts with a bistatic range error of 13.3 m, increasing to 29.9 m over the 900 s measurement. This bistatic range migration is a result of the two GPSDOs entering holdover with relative frequency offset. The relative phase of the radar nodes were evaluated by increasing the radar range-bin size such that the static target did not migrate range bins during the capture. The resultant phase series are plot in Figure 20b; A total phase excursion equivalent to 50.30 ns was observed during the capture. The FFO was again calculated for the measurement and can be found in Figure 20c. A mean offset of 5.87×10^{-11} was observed for the capture equivalent to Doppler and velocity errors of 142 mHz and of $1.8 \times 10^{-2}\ ms^{-1}$, respectively. This measurement provides a clear example of when the holdover performance of the GPSDOs are dominated by the initial frequency offset between LOs, as described in section 3.3.4. Unchecked, this frequency offset would result in a relative time error of 211 ns in 1-h, equivalent to a bistatic range migration of over 63 m. As a reminder, in these experiments the GPSDOs had not been left to reach optimal synchronisation to GPS. The mean FFO in this result is more than double the maximum FFO recorded between LNRCLOK-L6T devices in the lab measurements in section 3.3.3. If the GPSDOs had been left to reach optimal synchronisation to GPS, the relative frequency offset at the point of GPS denial would likely be a fraction of the offset observed in this measurement, meaning the holdover performance experienced would be considerably better. That considered, this example represents a worst case scenario.

6 | CONCLUSIONS

GNSS Disciplined Oscillators provide potentially ideal candidates for synchronisation MSRSs. However, as described in section 2, the radar's the bandwidth, central frequency and type of MSRS data fusion will stipulate the required synchronisation performance.

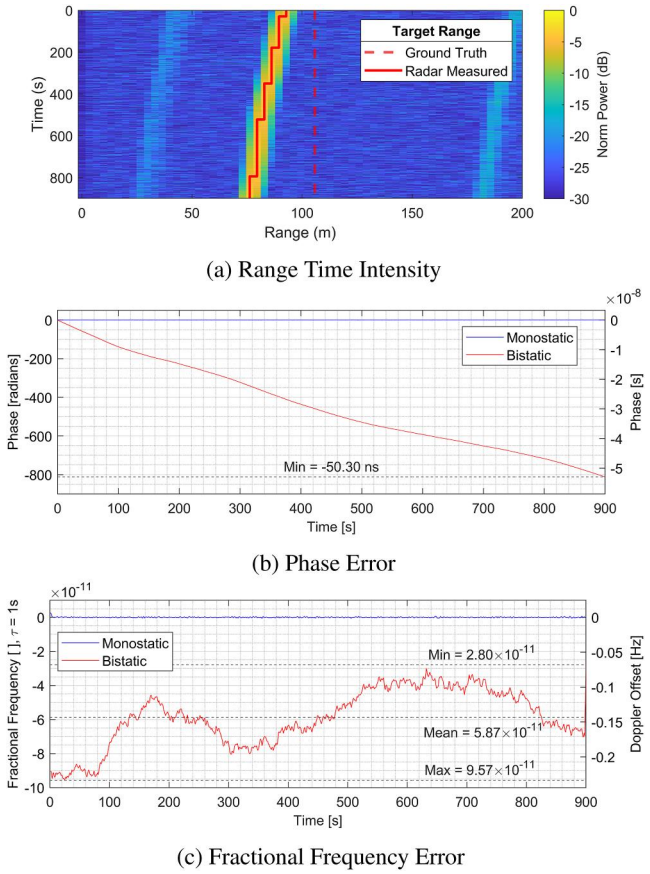

FIGURE 20 900 s measurement of a static target for long-term synchronisation analysis of the ARESTOR radar whilst disciplined to LNRCLOK-L6T GPSDOs in holdover, replicating Global Positioning System (GPS) denied operation. (a) Bistatic range time intensity plot. (b) Carrier phase of static target for monostatic and bistatic measurements. (c) Fractional Frequency error of carrier frequency for monostatic and bistatic measurements; low pass filtered and decimated to 1 Hz averaging period.

By comparing the relative timing accuracies of the GNSSDOs investigated in this work, it can be concluded that these one-way GNSSDOs would only be suitable for synchronisation of fully spatially coherent MSRSs with carrier frequencies up to 100 MHz. For MSRSs with higher carrier frequencies, fully coherent operation would not be possible without some form of signal processing phase correction. Some methods of phase correction have been proposed in Refs. [20, 44, 45], where static clutter or direct breakthrough are used to phase synchronise spatially separated nodes.

For short-term spatially coherent MSRS, with cooperative signal reception, it is highly likely the time accuracies between GNSSDOs will again limit their suitability. If some form of centralised multistatic data fusion is implemented, timing errors a fraction of the radars compressed pulse width are required. The best time accuracy of three GPSDOs pairs was the THUN-E devices, which provided a two-sigma of 4.28 ns, theoretically permitting centralised fusion for radars with bandwidths up to 23 MHz. If only decentralised fusion methods are required, the time accuracy requirements can be relaxed by an order of magnitude, making synchronisation of radars with bandwidths over 100 MHz theoretically possible using all three GNSSDO models. One should note, it is assumed mean node-to-node time offsets can be removed during a calibration step when assessing GNSSDO suitability MSRS synchronisation.

In short-term spatially coherent radars node-to-node frequency accuracy is required to allow accurate Doppler estimation, MTI processing and coherent integration. In the co-located GNSSDO lab measurements peak FFO of up to 4.20×10^{-11} were experienced, equivalent to a $1.26 \times 10^{-2}\ ms^{-1}$ velocity error. This is approximately a magnitude better than the requirements stated for the NeXtRAD system in Ref. [7]. It is also a fraction of the $6.19 \times 10^{-2}\ ms^{-1}$ velocity resolution of the ARESTOR system, as configured in section 5. The higher the central frequency of the radar the more stringent the requirement on node-to-node frequency accuracy, therefore it is summarised that these GNSSDOs would be suitable for synchronising short-term spatially coherent MSRS with carrier frequencies up to a few GHz.

In section 3.2.2 the relative stability of LOs were investigated where it was found the Rubidium based GPSDOs offer better longer-term stability, compared to the DOCXO GPSDOs. Therefore, in some cases, the Rubidium based GPSDOs will be able to provide time and frequency synchronisation for considerably greater duration's of GNSS denial than the DOCXO devices. However, as theorised in section 3.3.4 and later proven in practical radar measurements in section 5.3.2, the holdover performance of either LO is heavily dependent on the initial FFO between LOs when GNSS is lost.

The use of dual-frequency multi-GNSS timing receivers was found to marginally improve the timing and frequency synchronisation of co-located LNRCLOK GNSSDOs. In reality a bigger benefit will likely come from their resilience to GNSS denial from interference, jamming, spoofing or constellation failures. Using single-frequency single constellation GPS timing receivers presents a considerable single point of failure to a MSRS that depend on GPS for indirect synchronisation.

In a MSRS with greater than two nodes, additional STALOs will be required at each node. In this configuration, each pair of nodes will operate with a discrete relative time and frequency offset. Each time and frequency offset, will result in discrete bistatic range and Doppler velocity parameter estimation errors for bistatic sensing between nodes. For systems comprised of nodes that do not provide azimuth or elevation information, four transmit and receive pairs are required to perform localisation in three-dimensional space. In systems that have a greater number than four pairs, or that can individually localise targets at each node, it is highly likely that improved parameter estimation accuracy could be achieved by averaging out the error introduced by relative time and frequency offsets between nodes. Moreover, the performance of parameter estimation is also directly dependent on

the geometry made by the target between the transmitter and receiver [13]. The higher the number of nodes the greater the likelihood the target forms a favourable geometry with the system and subsequently provide better parameter estimation accuracy.

In summary, RadSync has been shown to provide wireless synchronisation of the ARESTOR radar and the ability for cooperative node-to-node signal reception. The GNSSDOs in this work would not permit fully coherent operation of the ARESTOR system, without some form of phase correction, limiting centralised fusion strategies to incoherent methods such as video fusion [3]. The time error between GNSSDOs will limit the waveform bandwidths—that could be used in the ARESTOR system if incoherent methods such as video fusion are implemented—to just over 20 MHz. If decentralised MSRS fusion strategies are used, the node-to-node timing accuracy requirements can be considerably relaxed, thus greater waveform bandwidths of over 100 MHz could be used.

AUTHOR CONTRIBUTIONS

PB was responsible for the study conception, data collection, analysis, and interpretation of the GNSSDO performance; In addition to the design and development of the RadSync synchronisation system. NP, CH and MR were responsible for the conception and development of the ARESTOR system and authored the description of the ARESTOR platform. All authors participated in the ARESTOR multistatic radar trials and helped draft, read, and approve the final manuscript.

ACKNOWLEDGEMENTS

The authors would like to acknowledge the UK Defence Science and Technology Laboratory and Engineering and Physical Sciences Research Council (EPSRC) for PhD sponsorship for research in to multistatic radar. The authors would also like to acknowledge the Defence and Security Accelerator, Air Force Office of Scientific Research, and EPSRC for the funding that supported the ARESTOR system development, and Leonardo UK Ltd for their support via the EPSRC Discovery-to-Use programme.

CONFLICT OF INTEREST STATEMENT

The authors whose names are listed above certify they have no conflicts of interest with any organisations or commercial entities with interest in the subject matter or research presented in the manuscript.

DATA AVAILABILITY STATEMENT

The data that support the findings of this study are available from the corresponding author upon reasonable request.

ORCID

Piers J. Beasley https://orcid.org/0000-0002-4879-6525
Nial Peters https://orcid.org/0000-0001-6817-6262
Colin Horne https://orcid.org/0000-0003-3529-2560
Matthew A. Ritchie https://orcid.org/0000-0001-8423-8064

REFERENCES

1. Baker, C., Hume, A.: Netted radar sensing. IEEE Aero. Electron. Syst. Mag. 18(2), 3–6 (2003). https://doi.org/10.1109/maes.2003.1183861
2. Boyle, R., Wasylkiwskyj, W.: Comparison of monostatic and bistatic bearing estimation performance for low RCS targets. IEEE Trans. Aero. Electron. Syst. 30(3), 962–968 (1994). https://doi.org/10.1109/7.303773
3. Chernyak, V.: Fundamentals of Multisite Radar Systems. Gordon and Breach Science Publishers (1998)
4. Weib, M.: Synchronisation of bistatic radar systems. In: IEEE International Geoscience and Remote Sensing Symposium, vol. 3, pp. 1750–1753 (2004)
5. Cliche, J.-F., Shillue, B.: Applications of control precision timing control for radioastronomy maintaining femtosecond synchronization in the atacama large millimeter array. IEEE Control Sys. Mag. 26(1), 19–26 (2006). https://doi.org/10.1109/mcs.2006.1580149
6. Lewis, S., Sandenbergh, J., Inggs, M.: Evaluating an off-the-shelf White Rabbit system to synchronise network radar via optic fibre. In: IEEE Radar Conference, pp. 1657–1662 (2017)
7. Lewis, S., Inggs, M.: Synchronisation of coherent netted radar using white rabbit compared with one-way multichannel GPSDOs. IEEE Trans. Aero. Electron. Syst. 57(3), 1413–1422 (2021). https://doi.org/10.1109/taes.2020.3043530
8. Inggs, M., Sandenbergh, J., Lewis, S.: Investigation of White Rabbit for synchronization and timing of netted radar. In: IEEE Radar Conference, pp. 214–217 (2015)
9. Lipiński, M., et al.: White rabbit: a PTP application for robust sub-nanosecond synchronization. In: IEEE International Symposium on Precision Clock Synchronization for Measurement, Control and Communication, pp. 25–30 (2011)
10. Dierikx, E.F., et al.: White Rabbit multi-point time distribution network. In: Joint Conference of the Euro. Frequency and Time Forum and IEEE Interenational Frequency Control Symposium, pp. 1–4 (2021)
11. Gilligan, J., et al.: White Rabbit time and frequency transfer over wireless millimeter-wave carriers. IEEE Trans. Ultrason. Ferroelectrics Freq. Control 67(9), 1946–1952 (2020). https://doi.org/10.1109/tuffc.2020.2989667
12. Griffiths, D., et al.: Direct signal synchronization for staring passive bistatic radar. In: International Conference on Radar System, vol. 2022, pp. 220–225 (2022)
13. Willis, N.: Bistatic Radar, 1 ed. SciTech (2005)
14. Lombardi, M.A.: Evaluating the frequency and time uncertainty of GPS disciplined oscillators and clocks. NCSLI Measure 11(3-4), 30–44 (2016). https://doi.org/10.1080/19315775.2017.1316696
15. Lombardi, M., Novick, A., Zhang, V.: Characterizing the performance of GPS disciplined oscillators with respect to UTC. In: IEEE Interenational Frequency Control Symposium and Exposition, pp. 677–684 (2005)
16. Sandenbergh, J., Inggs, M.: A summary of the results achieved by the GPS Disciplined References of the NetRAD and NeXtRAD multistatic radars. In: IEEE Radar Conference, pp. 1–6 (2019)
17. Sandenbergh, J., Inggs, M.: Synchronizing network radar using all-in-view GPS-disciplined oscillators. In: IEEE Radar Conference, pp. 1640–1645 (2017)
18. Sandenbergh, J., Inggs, M., Al-Ashwal, W.A.: Evaluation of coherent netted radar carrier stability while synchronised with GPS-disciplined oscillators. In: IEEE Radar Conference, pp. 1100–1105 (2011)
19. Sandenbergh, J., Inggs, M.: A common view GPSDO to synchronize netted radar. In: 2007 IET International Conference on Radar System, pp. 1–5 (2007)
20. Sandenbergh, J.: Synchronising Coherent Networked Radar Using Low-Cost GPS-Disciplined Oscillators. PhD Thesis. University of Cape Town (2019)
21. Sandenbergh, J., et al.: An adaptive distributed clock for radar networks. In: International Radar Conference, pp. 1–5 (2019)
22. Kirchner, D.: Two-way time transfer via communication satellites. Proc. IEEE 79(7), 983–990 (1991). https://doi.org/10.1109/5.84975
23. Beasley, P., Ritchie, M.: Multistatic radar synchronisation using COTS GPS disciplined oscillators. In: International Conference on Radar System, vol. 2022, pp. 429–434 (2022)

24. Jahangir, M., et al.: Development of quantum enabled staring radar with low phase noise. In: European Radar Conference, pp. 225–228 (2022)
25. Doerry, A.: Radar Receiver Oscillator Phase Noise (2018)
26. Goldman, S.: Phase Noise Analysis in Radar Systems Using Personal Computers. Wiley (1989)
27. Derham, T., et al.: Ambiguity functions for spatially coherent and incoherent multistatic radar. IEEE Trans. Aerospace Elec. Sys. 46(1), 230–245 (2010). https://doi.org/10.1109/taes.2010.5417159
28. Bovey, C.K., Horne, C.P.: Synchronization aspects for bistatic radars. In: International Radar Conference, pp. 22–25 (1987)
29. Auterman, J.: Phase stability requirements for a bistatic SAR system. IEEE Int. Radar Conf., 48–52 (1984)
30. Riley, W.: Handbook of frequency stability analysis. Inside NIST 1065, 1–123 (2007)
31. Lewis, L.: An introduction to frequency standards. Proc. IEEE 79(7), 927–935 (1991). https://doi.org/10.1109/5.84969
32. Marlow, B.L.S., Scherer, D.R.: A review of commercial and emerging atomic frequency standards. IEEE Trans. Ultrason. Ferroelectrics Freq. Control 68(6), 2007–2022 (2021). https://doi.org/10.1109/tuffc.2021.3049713
33. Renesas: AN-815: Understanding Jitter Units. Renesas Electronics Corporation (2014)
34. Kaplan, E., Hegarty, C.: Understanding GPS/GNSS: Principles and Applications, ed. Artech House (2017)
35. Beasley, P.J., Ritchie, M.A., bladerad: Development of an active and passive, multistatic enabled, radar system. In: European Radar Conference, pp. 98–101 (2022)
36. Beasley, P.J., Ritchie, M.A.: Multi-band hybrid active-passive radar sensor fusion. In: In Press, IEEE Radar Conference (2023)
37. Ritchie, M., Peters, N., Horne, C.: Joint active passive sensing using a radio frequency System-on-a-Chip based sensor. In: International Radar Symposium, pp. 130–135 (2022)
38. Peters, N.J., et al.: Modular multi-channel RFSoC system expansion and array design. In: IEEE Radar Confernational. San Antonio (2023)
39. Alhuwaimel, S., et al.: First measurements with NeXtRAD, a polarimetric X/L band radar network. In: IEEE Radar Conference, pp. 1663–1668 (2017)
40. Inggs, M., et al.: Report on the 2018 trials of the multistatic NeXtRAD dual band polarimetric radar. In: IEEE Radar Conference, pp. 1–6 (2019)
41. Peters, N., Horne, C., Ritchie, M.A.: ARESTOR: a multi-role RF sensor based on the Xilinx RFSoC. In: 2021 18th European Radar Conference (EuRAD), pp. 102–105 (2022)
42. Dhulashia, D., et al.: Multi-frequency radar micro-Doppler based classification of micro-drone payload weight. Front. Signal Process. 1 (2021). https://doi.org/10.3389/frsip.2021.781777
43. Temiz, M., et al.: An experimental study of radar-centric transmission for integrated sensing and communications. IEEE Trans. Microw. Theor. Tech. 71(7), 1–14 (2023). https://doi.org/10.1109/tmtt.2023.3234309
44. Al-Ashwal, W.A., Griffiths, H.D.: Preliminary analysis of monostatic and bistatic Doppler signature of small maritime target. In: International Conference on Radar, pp. 494–499 (2013)
45. Al-Ashwal, W.: Measurement and Modelling of Bistatic Sea Clutter. PhD Thesis. University College London (2011)

How to cite this article: Beasley, P.J., et al.: Global Navigation Satellite Systems disciplined oscillator synchronisation of multistatic radar. IET Radar Sonar Navig. 1–18 (2023). https://doi.org/10.1049/rsn2.12475